



Efficient room-temperature solid-state lithium ion conductors enabled by mixed-graft block copolymer architectures

Xiaoyu Ji^{a,b}, Mengxue Cao^a, Xiaowei Fu^{a,c}, Ruiqi Liang^a, An N. Le^a, Qiuting Zhang^e, Mingjiang Zhong^{a,d,*}

^a Department of Chemical and Environmental Engineering, Yale University, New Haven, CT 06511, USA

^b Science and Technology on Advanced Ceramic Fibers and Composites Laboratory, College of Aerospace Science and Engineering, National University of Defense Technology, Changsha 410073, China

^c State Key Laboratory of Polymer Materials Engineering, Polymer Research Institute of Sichuan University, Chengdu 610065, China

^d Department of Chemistry, Yale University, New Haven, CT 06511, USA

^e Department of Molecular, Cellular, and Developmental Biology, Yale University, New Haven, CT 06511, USA

Keywords: Graft copolymers, Room-temperature lithium battery, Solid-state electrolytes

Fast lithium ion (Li^+) transport in solid-state polymer-matrix conductors is in desperate demand in a wide range of room-temperature scenarios but remains a formidable challenge. Herein, we designed a class of solid-state electrolytes based on mixed-graft block copolymers (mGBCPs) containing short poly(ethylene oxide) (PEO) and polydimethylsiloxane (PDMS) side chains. The strong immiscibility of PEO and PDMS resulted in the formation of ordered phase-separated nanostructures. Diverse morphologies, including double gyroids, hexagonally perforated lamellae, hexagonally packed cylinders, and lamellae, were observed at different volume fractions of PEO/PDMS blocks. The impact of chain mobility of PEO on Li^+ transport was investigated by varying the length of PEO side chains and blending with free PEO chains. We demonstrated that physically blending mGBCPs with free amorphous PEO chains significantly facilitated the Li^+ conduction, and a solid-state electrolyte with room-temperature conductivity up to 2.0×10^{-4} S/cm was prepared.

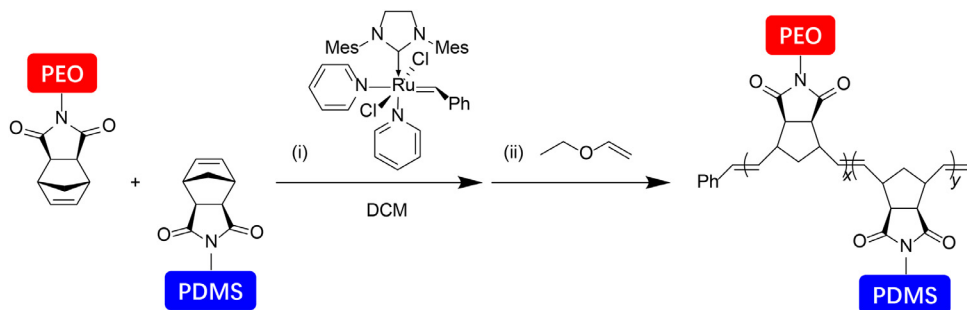
The superior economic benefits and sustainability of rechargeable batteries enable their widespread use as energy storage devices in electric vehicles, grid-level storage, and portable electronics [1–3]. Lithium batteries, one of the most

intensively studied rechargeable batteries, typically contain highly conductive liquid-phase electrolytes to ensure their high performance. Unfortunately, the organic liquid electrolytes present safety concerns due to their flammability and risk of leakage [4]. Furthermore, short circuit caused by Li dendrite growth during battery cycling cannot readily be prevented in the liquid medium [5]. In this regard, solid-state electrolytes provide an alternative class of ion-conductive materials for the

* Corresponding author at: Department of Chemical and Environmental Engineering, Yale University, New Haven, CT 06511, USA.

E-mail address: mingjiang.zhong@yale.edu (M. Zhong).

Received 3 August 2020; Received in revised form 30 August 2020; Accepted 5 September 2020

**Scheme 1**

Synthesis of mGBCPs from norbornene-monofunctionalized PEO and PDMS macromonomers.

fabrication of lithium batteries with enhanced security, durability, and portability [6–10].

Poly(ethylene oxide) (PEO) is one of the most widely applied matrix materials for solid-state electrolytes for Li^+ conduction due to its high dielectric constant, desirable solvation site connectivity, versatile processability, and high cost efficiency [11–14]. An operating temperature above the melting temperature (T_m) of PEO is often required to eliminate PEO crystallization and slow chain motions that hinder the Li^+ transport. However, such temperatures also diminish the solid feature of the electrolytes. While the mechanical strength can be improved in self-assembled block copolymers (BCPs) containing PEO and a complementary “hard” block [15–19], the high molecular weight (MW) of PEO needed for BCP nanophase separation is accompanied by low chain mobility and a high T_m [20], which inevitably translates into high operating temperatures, e.g., above 60 °C. Another prevailing method that enhances the mechanical strength of PEO melts involves the formation of end-linked PEO networks, albeit the thermosetting nature of the covalently crosslinked electrolytes limits their processability and recyclability [21–23]. Design of processable solid-state PEO-based electrolytes that function at room temperature is in demand for a broad range of applications but remains an unmet challenge [24].

We recently reported a mixed-graft block copolymer (mGBCP) architecture that enabled nanophase separation between side chain blocks with unusually low molecular weights [25,26]. The mGBCPs were synthesized through ring-opening metathesis polymerization (ROMP) of a branched macromonomer (BMM) – a norbornene molecule covalently tethered with two distinct polymeric side chains [27]. The two blocks that dictated the nanostructures were preorganized in a pseudo-alternating sequence upon ROMP. Thus, a disordered BMM with a low MW in each block could be converted into an ordered nanostructure due to the backbone-stabilized interface and suppressed mixing entropy in the mGBCP architecture. The thermomechanical properties of mGBCPs could be independently tuned by varying the backbone length with minimal influence on the nanostructures. Taking advantage of the mGBCP architecture, we hypothesized that an mGBCP with short-chain PEO as one of the blocks could be designed for a room-temperature Li^+ -conductive material with desirable mechanical strength.

In this work, a simplified synthetic route (Scheme 1) – random copolymerization of norbornene-monofunctionalized

Table 1**Composition of as-synthesized $(\text{PEO750})_x-r-(\text{PDMS1k})_y$, mGBCPs.**

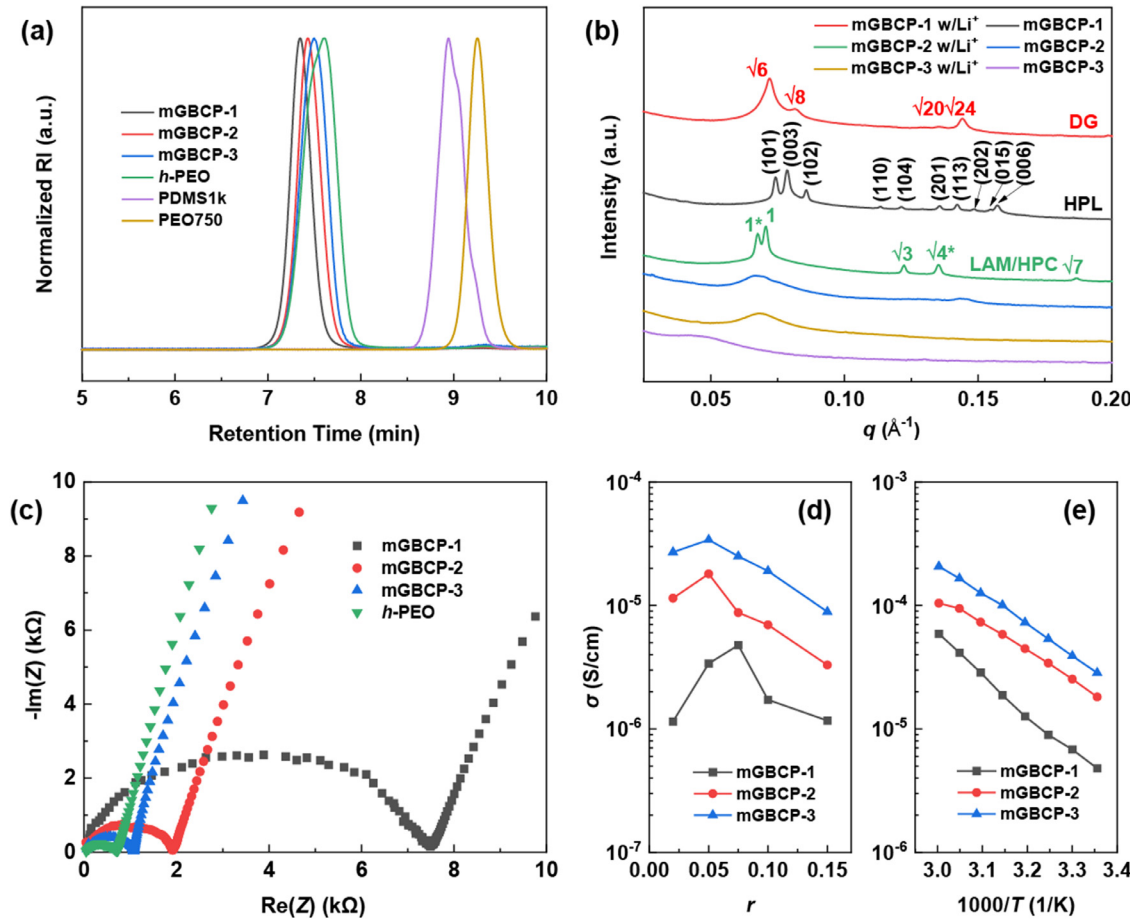
Sample	Composition	M_n^a (kDa)	D^a	φ_{PEO}^b
mGBCP-1	$(\text{PEO750})_{25}-r-(\text{PDMS1k})_{25}$	26.0	1.04	0.42
mGBCP-2	$(\text{PEO750})_{35}-r-(\text{PDMS1k})_{15}$	22.0	1.04	0.63
mGBCP-3	$(\text{PEO750})_{43}-r-(\text{PDMS1k})_7$	20.7	1.05	0.81
<i>h</i> -PEO	$(\text{PEO750})_{50}$	17.7	1.08	1.00

^a Determined by gel permeation chromatography (GPC) with polystyrene as the calibration standard.

^b Calculated based on nuclear magnetic resonance (NMR) spectra.

linear macromonomers (LMMs) [28] of PEO with MW of 750 Da, referred to as PEO750, and polydimethylsiloxane (PDMS) with MW of 1000 Da, i.e., PDMS1k, was employed to create a series of mGBCP-based solid-state electrolytes that function at room temperature. The facile synthesis and reduced steric hindrance of the LMMs, compared to BMMs, provided a synthetic platform towards mGBCPs with significantly improved scalability. Moreover, the diversity of the resulting nanostructures was readily achieved by varying the volume fraction (φ) of the two blocks, i.e., the feed ratio of the two LMMs. While polymers with a relatively high glass transition temperature (T_g), e.g., polystyrene (PSt) and poly(lactic acid) (PLA), possess the potential to attain higher mechanical strength than PDMS, the low Flory–Huggins parameters (χ) of PSt and PLA with PEO (Table S1) [29–31] will lead to the formation of disordered phases in corresponding mGBCPs. The strong incompatibility between PEO and PDMS ensures their nanophase separation to form nanochannels in mGBCPs, and the low MW of PEO750 provides a crystallization-free fluid phase for fast Li^+ conduction at room temperature. After partially replacing the tethered PEO side chains with free PEO chains, a room-temperature Li^+ conductivity as high as 2.0×10^{-4} S/cm was achieved without compromising the mechanical strength of the solid-state electrolytes.

$(\text{PEO750})_x-r-(\text{PDMS1k})_y$, mGBCPs with a fixed overall degree of polymerization (DP) ($x + y = 50$) of the backbone were synthesized, as summarized in Table 1. A graft polymer prepared from the homopolymerization of PEO750 with the same backbone DP was used as a reference and denoted as *h*-PEO. All mGBCPs were synthesized with nearly quantitative conversion of both LMMs and low dispersity ($D < 1.10$) (Fig. 1a). The polymers were blended with lithium bis(trifluoromethanesulfonyl)imide

**Fig. 1**

(a) GPC traces of macromonomers, *h*-PEO, and mGBCPs; (b) SAXS profiles of mGBCPs with and without LiTFSI ($r = 0.05$); (c) Nyquist plots of the mGBCP electrolytes with various compositions ($T = 25^\circ\text{C}$); Plots of conductivity (σ) vs. (d) Li^+ concentrations ($T = 25^\circ\text{C}$) and (e) inverse temperature.

(LiTFSI) in tetrahydrofuran at varied molar ratios (r) of Li^+ to the $-\text{CH}_2-\text{CH}_2-\text{O}-$ repeating units of PEO, followed by slow solvent evaporation for further structural, electrochemical, and rheological characterization.

Data obtained from small-angle X-ray scattering (SAXS) experiments revealed the diverse morphologies with the variation of φ and r (Fig. 1b, S10-12). mGBCP-1 with φ_{PEO} of 0.42 displayed a hexagonally perforated lamellar (HPL) structure. The scattering pattern was assigned to a $\text{R}\bar{3}\text{m}$ structure with lattice parameters of $a = b = 10.5 \text{ nm}$, $c = 24.0 \text{ nm}$ and an ABCABC trigonal stacking (Table S2) [32,33]. The fact that the linear BCP PEO750-*b*-PDMS1k with a similar φ_{PEO} to mGBCP-1 has a disordered morphology (Fig. S16) [25] indicates the critical role of the mGBCP architecture in facilitating ordered phase separation [26]. A transition to a bicontinuous double-gyroidal (DG) structure was observed in mGBCP-1 upon the addition of LiTFSI ($r = 0.05$). This Li^+ -induced change in self-assembly behaviors could be attributed to the alteration of both the chemical nature and the volume fraction of the PEO phase. Due to the higher dielectric constant (ϵ) of PEO ($\epsilon_{\text{PEO}} = 4-8$ [34,35] vs $\epsilon_{\text{PDMS}} = 2-3$ [36,37]) and specific coordination interactions between ether oxygens and Li^+ ions [38,39], Li^+ ions are preferentially enriched in the PEO domains, thereby further increasing the incompatibility of the

two phases [40]. In parallel, the additional volume of LiTFSI and chain stretching arising from coordination between PEO and Lithium salt can lead to a variation in the volume fraction as well [41]. The disordered neat mGBCP-2 ($\varphi_{\text{PEO}} = 0.63$) also underwent a Li^+ -induced morphological transition at $r = 0.05$ to a coexisting phase of lamellae (LAM) and hexagonally packed cylinders (HPC). Although blending with LiTFSI further increased the φ_{PEO} in mGBCP-2, this disorder-to-order transition indicated that the enhanced incompatibility between PDMS and Li^+ -enriched PEO enabled the phase separation. However, mGBCP-3 remained disordered (DIS) after blending with LiTFSI due to its high compositional asymmetry ($\varphi_{\text{PEO}} = 0.81$).

The crystallinity of PEO750 in mGBCP electrolytes was evaluated using differential scanning calorimetry (DSC) (Fig. S18, 19). Neat mGBCPs exhibited an endothermic peak at 25°C during heating, which corresponded to the T_m of PEO750. The characteristic peaks of melting and crystallization were both missing in mGBCP electrolytes with various r from 0.02 to 0.15 within the temperature range from -30 to 150°C , indicating that PEO chains in mGBCP electrolytes are amorphous due to their interaction with Li^+ . Calorimetric signals that corresponded to T_g were not detected across the entire temperature sweep window in both mGBCPs and their Li^+ -blended samples.

Table 2

Morphologies and ionic conductivities of the mGBCP electrolytes at 25 °C and $r = 0.05$.

Sample	Morphology	σ_0^a (S/cm)	σ (S/cm)
mGBCP-1	DG	1.4×10^{-5}	3.3×10^{-6}
mGBCP-2	LAM/HPC	3.1×10^{-5}	1.8×10^{-5}
mGBCP-3	DIS	4.0×10^{-5}	3.4×10^{-5}

^a σ_0 , theoretical value of ionic conductivity calculated by Eq. (1) with $\sigma_c = 4.9 \times 10^{-5}$ S/cm.

Electrochemical impedance spectroscopy (EIS) was used to evaluate the ionic conductivity by casting a polymer/LiTFSI film sandwiched between two standard stainless steel blocking electrodes. Nyquist plots of mGBCP electrolytes and the r -dependent conductivities are summarized in Fig. 1c and d and S20–25. Conductivities (σ) of all mGBCP electrolytes approached the highest value at moderate blending ratios of $r = 0.050$ –0.075. At low lithium salt loadings, conductivity increases with $[Li^+]$ due to an increased number of charge carriers. After Li^+ saturates the binding sites of PEO, further increase of $[Li^+]$ reduces the PEO chain mobility due to transient ionic crosslinking [42].

Apart from $[Li^+]$, the volume fraction and morphology also showed a remarkable influence on the ionic conductivity of BCPs as described in Eq. (1) [43,44].

$$\sigma_{BCP} = f\varphi_c\sigma_c \quad (1)$$

where φ_c and σ_c are the volume fraction and the intrinsic conductivity of the conductive phase, respectively, and f is a morphology factor that has theoretical values of 1/3, 2/3, and 1 for 1D continuous HPC, 2D continuous LAM, and 3D continuous conductive phases, respectively. At $r = 0.05$, all three mGBCP electrolytes formed morphologies with 3D continuous PEO domains, i.e., DG phase (mGBCP-1), coexistence of LAM and HPC with PEO as the majority (mGBCP-2), and PEO-continuous disordered phase (mGBCP-3). Therefore, the f value is theoretically equal to 1 for the three mGBCP electrolytes. σ_c was then determined using the conductivity of *h*-PEO, with the value of 4.9×10^{-5} S/cm at $r = 0.05$.

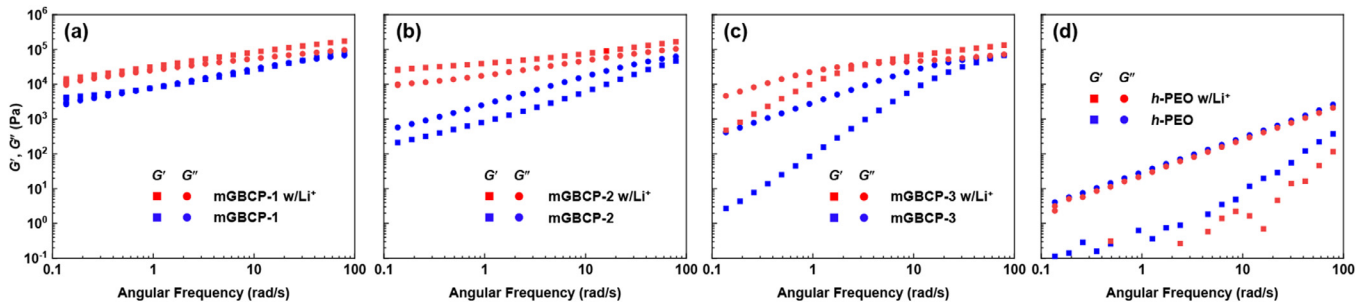
With the φ_{PEO} increasing from 0.42 to 0.81, the conductivity of mGBCP electrolytes at their optimal r increased from 3.3×10^{-6} S/cm (mGBCP-1) to 3.4×10^{-5} S/cm (mGBCP-3). However, the measured conductivities of mGBCP electrolytes were all lower than those calculated by Eq. (1), as summarized in Table 2. This discrepancy could be attributed to the low-surface-energy PDMS block that preferentially wet the stainless steel electrodes, resulting in an insulating layer between conductive PEO domains and electrodes [45,46]. The larger difference between σ and σ_0 in mGBCPs with higher φ_{PDMS} (from mGBCP-3 to mGBCP-1) further demonstrated the negative impact of the preferential electrode wetting by the PDMS block, which could potentially be eliminated by employing PEO-modified electrodes [45].

The influence of temperature on morphology and ionic conductivity was further investigated at temperatures ranging from room temperature to 60 °C. Variable temperature SAXS profiles (Figs. S13–15) indicated no morphological change within

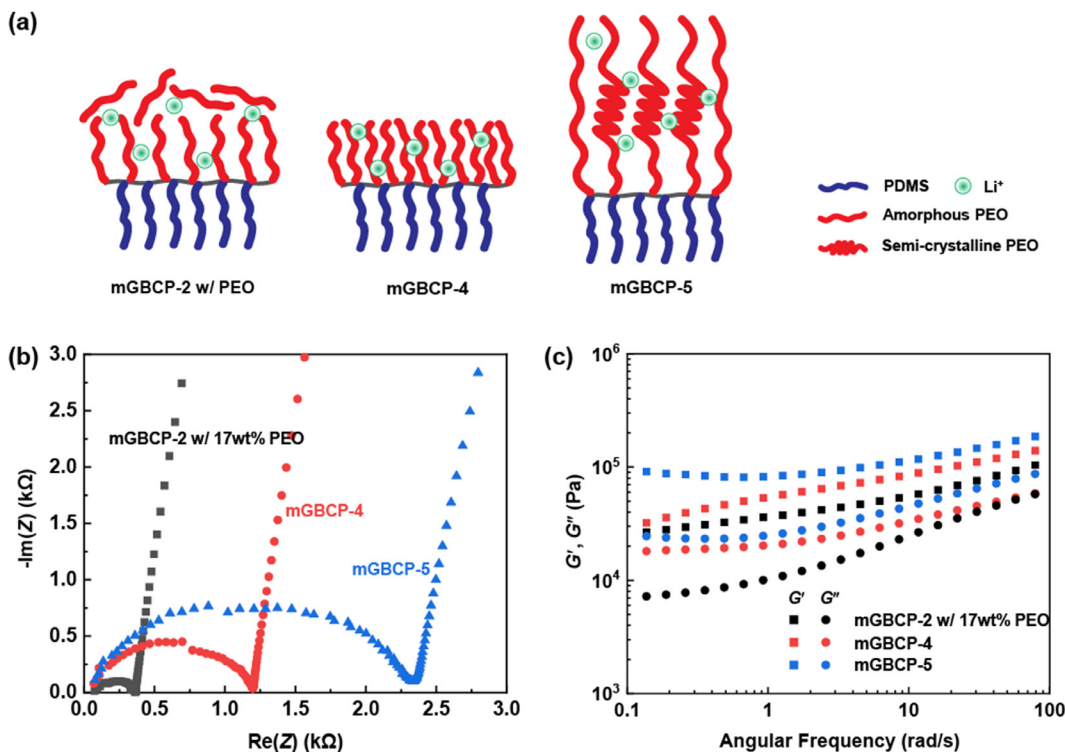
this temperature range. As shown in Fig. 1e and Fig. S26–31, the conductivities of mGBCP electrolytes increased monotonically with temperature. This temperature effect is consistent with the intrinsic relation of ionic conductivity with charge carrier concentration (c) and ion mobility (μ): $\sigma = \mu \times c$; elevated temperature facilitates the motion of the polymer chains and the Li^+ dissociation, leading to higher μ and c , respectively [24].

Rheological experiments based on the oscillatory frequency sweep method were conducted to calculate the storage (G') and loss (G'') moduli of both neat and LiTFSI-containing mGBCPs with $r = 0.05$ (Fig. 2). Introducing a liquid-like PDMS complementary block provided more elastic materials, i.e., higher G' , compared to *h*-PEO. This enhanced solid feature was further amplified after LiTFSI was dissolved in the mGBCPs. For instance, the liquid-like and disordered mGBCP-2 with higher G'' than G' ($\tan\delta > 1$) became a viscoelastic solid after Li^+ addition ($r = 0.05$), with G' in the range of 10^4 – 10^5 Pa (Fig. 2b), approximately 3–4 orders of magnitude higher than the liquid-like *h*-PEO (Fig. 2d) and 100 times higher than the linear BCP of PEO750-*b*-PDMS1k with the same Li^+ content (Figure S34). The enhancement in the mechanical strength could be ascribed to a cooperative effect of Li^+ -mediated physical crosslinking of PEO chains and covalent mGBCP backbone-stabilized ordered nanostructured interfaces. These room-temperature Li^+ -conductive mGBCP electrolytes with enhanced mechanical strength have advantages in suppressing Li dendrite formation in a rechargeable battery, enabling a high-rate and high-capacity lithium metal cycling [47–49].

To investigate the impact of the chain mobility on the Li^+ conductivity, we compared three types of mGBCP-based electrolytes with consistent volume fractions of PEO ($\varphi_{PEO} = 0.71$ –0.72) but distinct PEO components, including mGBCP-2 physically blended with free PEO750 chains (17 wt%), (PEO750)₃₈-*r*-(PDMS1k)₁₂, and (PEO2k)₁₈-*r*-(PDMS1k)₁₂ (Fig. 3a). The latter two samples are referred to as mGBCP-4 and mGBCP-5, respectively. Evidenced by the SAXS profiles (Figure S17), the first two electrolytes with $r = 0.05$ shared the same morphology of HPC, and therefore their difference in conductivities would be predominantly influenced by PEO chain mobility. Adding free PEO750 into the mGBCP drastically improved the room-temperature Li^+ conductivity from 3.0×10^{-5} S/cm for mGBCP-4 to 1.0×10^{-4} S/cm for PEO750-blended mGBCP-2 (Fig. 3b). With consistent volume fractions and morphology, the high conductivity in mGBCP-2 with free PEO750 chains was partially achieved by releasing part of the PEO side chains that were immobilized in mGBCP-4 at one of their two chain ends to an unbound state. Moreover, the conductivity could also benefit from reduced intersegmental repulsion in free PEO chains, which has been demonstrated in linear BCP electrolyte systems [50–52]. The rheological studies (Fig. 3c) demonstrated similar viscoelastic solid features in the two samples, with G' in the range of 10^4 – 10^5 Pa. A slight decrease of G' from mGBCP-4 to PEO750-blended mGBCP-2 could be attributed to the increased free volume originating from the introduction of free PEO chains to replace the tethered mGBCP side chains. The added free PEO750 component in the blended mGBCP-2 electrolytes served as a plasticizer that facilitated the ion transport [53,54] but did not alter the nanostructures of the viscoelastic solid. While mGBCP-5

**Fig. 2**

Frequency sweeps of mGBCPs and *h*-PEO with ($r = 0.05$) and without LiTFSI: (a) mGBCP-1; (b) mGBCP-2; (c) mGBCP-3; (d) *h*-PEO.

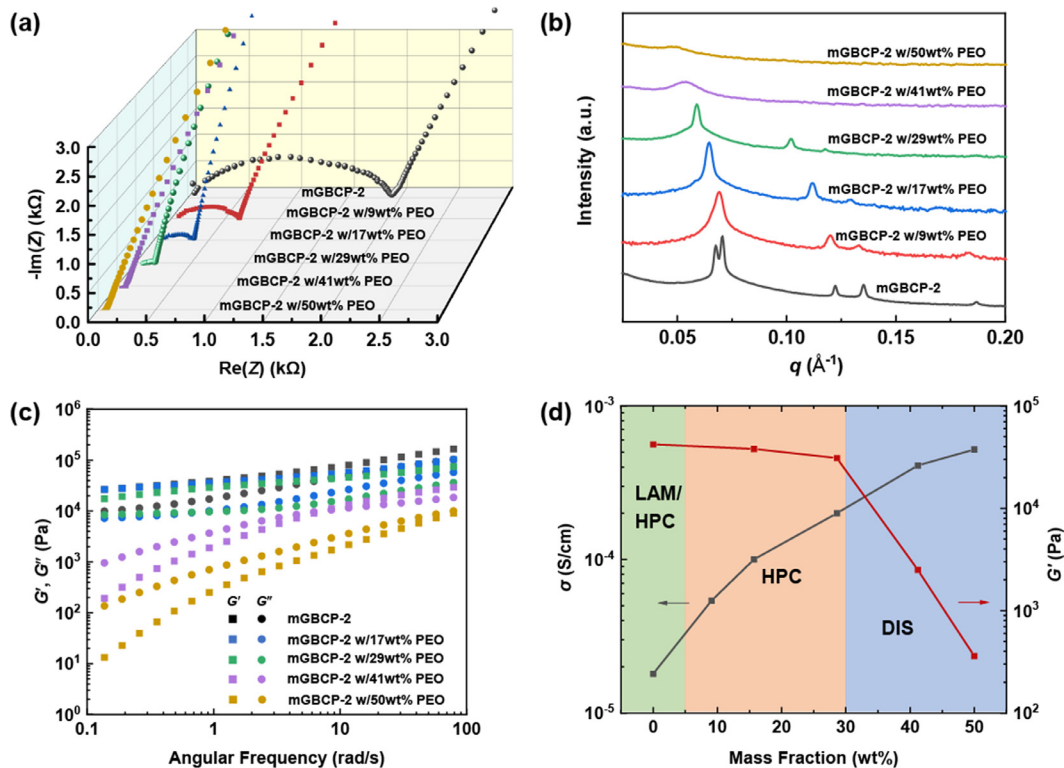
**Fig. 3**

(a) Schematic illustrations of three types of mGBCP-based Li^+ conductors with $\varphi_{\text{PEO}} = 0.71\text{--}0.72$; (b) Nyquist plots ($T = 25^\circ\text{C}$) of mGBCP-based Li^+ conductors ($r = 0.05$) and (c) rheological frequency sweeps. mGBCP-4: $(\text{PEO750})_{38}\text{-}r(\text{PDMS1k})_{12}$. mGBCP-5: $(\text{PEO2k})_{18}\text{-}r(\text{PDMS1k})_{12}$.

possessed the highest G' among the three samples, its higher crystallinity and the lower mobility of PEO2k that contributed to the high G' provided Li^+ with a less dynamic solvation environment and led to a Li^+ conductivity approximately an order of magnitude lower than that of the blended mGBCP-2. These results are consistent with recently studied ABA tri-block bottlebrush copolymers containing PEO2k side chains with φ_{PEO} of 0.75–0.77, showing room-temperature Li^+ conductivity of *ca.* $2.0 \times 10^{-5} \text{ S/cm}$ and storage modulus of $10^4\text{--}10^5 \text{ Pa}$ at 45°C [55].

The role of free PEO chains in the enhancement of the ionic conductivity was further manifested by the systematic investigation of the Li^+ transport behaviors in mGBCP-2 blended with varied mass fractions of free PEO750. Nyquist plots (Fig. 4a) display a monotonically increasing trend of the Li^+ conductivity

with the mass fraction of free PEO750 chains. With the mass fraction below 30 wt%, an ordered nanostructure with LAM/HPC or HPC morphology (Fig. 4b) was observed in a viscoelastic solid ($G' > G''$) (Fig. 4c). The highest conductivity of $2.0 \times 10^{-4} \text{ S/cm}$ at room temperature was achieved in this regime with nearly unchanged storage modulus ($G' > 3 \times 10^4 \text{ Pa}$) (Fig. 4d). These free PEO-blended mGBCP polyelectrolytes exhibited superior room-temperature conductivity compared to previously reported solid-state electrolytes derived from bottlebrush copolymers and brush-arm star polymers comprised of PEO side chains with MWs from 550 to 2000 Da [56,57]. While further increasing the fraction of free PEO750 continued to improve the conductivity, the electrolyte transitioned from a nanostructurally ordered solid sharply to a viscoelastic liquid with disordered phases when

**Fig. 4**

(a) Nyquist plots, (b) SAXS profiles, and (c) rheological frequency sweeps of mGBCP-2-based Li⁺ conductors with various mass fractions of the free PEO750 chains at $r = 0.05$; (d) Diagram showing the relationship between conductivity, storage modulus, and mass fraction of the free PEO750 chains.

the fraction was above 30 wt% (Fig. 4c and d). The ordered nanostructure not only provides channels for ion transport but also plays a key role in the mechanical performance of the mGBCP electrolytes.

Conclusions

In summary, we developed a facile synthetic approach to solid-state Li⁺-conductive electrolytes based on mGBCP architectures and explored the impact of chain mobility on Li⁺ transport efficiency. Ionic conductivity as high as 2.0×10^{-4} S/cm was achieved at room temperature. While the neat *h*-PEO and linear copolymer counterparts exhibit a liquid-like character, the mGBCP-based conductors possess viscoelastic-solid-like features and an elevated storage modulus in the range of 10^4 – 10^5 Pa. Conductive phases based on crystalline long side chains (PEO2k), amorphous short side chains (PEO750), and combinations of tethered side chains on mGBCP backbone and free chains (PEO750) were studied with identical volume fraction and morphology. Ionic conductivity was optimized through increasing chain mobility of the conductive PEO phase by either suppressing PEO crystallization or releasing the interface restriction of PEO chains. Furthermore, blending free PEO chains can efficiently facilitate the Li⁺ transport in a wide range of blending fraction with negligible sacrifice of the mechanical strength.

Declaration of Competing Interest

There are no conflicts to declare.

Acknowledgments

This work was financially supported by the National Science Foundation through Grant No. DMR-2003875. X.J. and X.E. are thankful for the financial support from the China Scholarship Council (No. 201903170199 and No. 201706240130, respectively) for their visits at Yale University. A.N.L. thanks the National Science Foundation Graduate Research Fellowships for their support. The authors thank Prof. Chinedum Osuji, Dr. Changyeon Lee, and Ruiqi Dong at the University of Pennsylvania for DSC characterization. The authors also thank Prof. Jing Yan at Yale University for access to his rheometer. The research used resources of the CMS beamline (11-BM) of the National Synchrotron Light Source II, a U.S. Department of Energy (DOE) Office of Science User Facility operated for the DOE Office of Science by Brookhaven National Laboratory (BNL) under Contract No. DE-SC0012704. The authors also thank Dr. Ruipeng Li (BNL) and Dr. Brandon Q. Mercado (Yale) for their technical assistance with SAXS measurements during the COVID-19 pandemic.

Supplementary materials

Supplementary material associated with this article can be found, in the online version, at doi:10.1016/j.giant.2020.100027.

References

- [1] M. Armand, J.-M. Tarascon, Building better batteries, *Nature* 451 (7179) (2008) 652–657.
- [2] S. Chu, A. Majumdar, Opportunities and challenges for a sustainable energy future, *Nature* 488 (7411) (2012) 294–303.
- [3] D. Larcher, J.M. Tarascon, Towards greener and more sustainable batteries for electrical energy storage, *Nat. Chem.* 7 (1) (2015) 19–29.
- [4] K. Xu, Nonaqueous liquid electrolytes for lithium-based rechargeable batteries, *Chem. Rev.* 104 (10) (2004) 4303–4418.
- [5] P. Bai, J. Li, F.R. Brushett, M.Z. Bazant, Transition of lithium growth mechanisms in liquid electrolytes, *Energy Environ. Sci.* 9 (10) (2016) 3221–3229.
- [6] A. Manthiram, X.W. Yu, S.F. Wang, Lithium battery chemistries enabled by solid-state electrolytes, *Nat. Rev. Mater.* 2 (4) (2017).
- [7] J. Mindemark, M.J. Lacey, T. Bowden, D. Brandell, Beyond PEO—Alternative host materials for Li⁺-conducting solid polymer electrolytes, *Prog. Polym. Sci.* 81 (2018) 114–143.
- [8] Q. Zhou, J. Ma, S. Dong, X. Li, G. Cui, Intermolecular chemistry in solid polymer electrolytes for high-energy-density lithium batteries, *Adv. Mater.* 31 (50) (2019) 190209.
- [9] Q. Zhao, S. Stalin, C.-Z. Zhao, L.A. Archer, Designing solid-state electrolytes for safe, energy-dense batteries, *Nat. Rev. Mater.* 5 (3) (2020) 229–252.
- [10] K.J. Harry, D.T. Hallinan, D.Y. Parkinson, A.A. MacDowell, N.P. Balsara, Detection of subsurface structures underneath dendrites formed on cycled lithium metal electrodes, *Nat. Mater.* 13 (1) (2014) 69–73.
- [11] P.V. Wright, Electrical conductivity in ionic complexes of poly(ethylene oxide), *Br. Polym. J.* 7 (5) (1975) 319–327.
- [12] P. Vashishta, J.N. Mundy, *Fast Ion Transport in Solids: Electrodes and Electrolytes*, Elsevier North Holland, Inc, United States, 1979.
- [13] Z. Gadjourova, Y.G. Andreev, D.P. Tunstall, P.G. Bruce, Ionic conductivity in crystalline polymer electrolytes, *Nature* 412 (6846) (2001) 520–523.
- [14] Z. Xue, D. He, X. Xie, Poly (ethylene oxide)-based electrolytes for lithium-ion batteries, *J. Mater. Chem. A* 3 (38) (2015) 19218–19253.
- [15] G. Stone, S. Mullin, A. Teran, D. Hallinan, A. Minor, A. Hexemer, N. Balsara, Resolution of the modulus versus adhesion dilemma in solid polymer electrolytes for rechargeable lithium metal batteries, *J. Electrochem. Soc.* 159 (3) (2012) A222–A227.
- [16] R. Bouchet, S. Maria, R. Meziane, A. Aboulaich, L. Lienafa, J.P. Bonnet, T.N.T. Phan, D. Bertin, D. Gigmes, D. Devaux, R. Denoyel, M. Armand, Single-ion BAB triblock copolymers as highly efficient electrolytes for lithium-metal batteries, *Nat. Mater.* 12 (5) (2013) 452–457.
- [17] I. Gurevitch, R. Buonsanti, A.A. Teran, B. Gludovatz, R.O. Ritchie, J. Cabana, N.P. Balsara, Nanocomposites of titanium dioxide and polystyrene-poly (ethylene oxide) block copolymer as solid-state electrolytes for lithium metal batteries, *J. Electrochem. Soc.* 160 (9) (2013) A1611–A1617.
- [18] G.K. Sethi, X. Jiang, R. Chakraborty, W.S. Loo, I. Villaluenga, N.P. Balsara, Anomalous self-assembly and ion transport in nanostructured organic-inorganic solid electrolytes, *ACS Macro Lett.* 7 (9) (2018) 1056–1061.
- [19] X.H. Dong, B. Ni, M. Huang, C.H. Hsu, R. Bai, W.B. Zhang, A.C. Shi, S.Z. Cheng, Molecular-curvature-induced spontaneous formation of curved and concentric lamellae through nucleation, *Angew. Chem. Int. Ed.* 55 (7) (2016) 2459–2463.
- [20] L. Zhu, S.Z. Cheng, B.H. Calhoun, Q. Ge, R.P. Quirk, E.L. Thomas, B.S. Hsiao, F. Yeh, B. Lotz, Crystallization temperature-dependent crystal orientations within nanoscale confined lamellae of a self-assembled crystalline–amorphous diblock copolymer, *J. Am. Chem. Soc.* 122 (25) (2000) 5957–5967.
- [21] S. Choudhury, R. Mangal, A. Agrawal, L.A. Archer, A highly reversible room-temperature lithium metal battery based on crosslinked hairy nanoparticles, *Nat. Commun.* 6 (1) (2015) 10101.
- [22] Q. Pan, D.M. Smith, H. Qi, S. Wang, C.Y. Li, Hybrid electrolytes with controlled network structures for lithium metal batteries, *Adv. Mater.* 27 (39) (2015) 5995–6001.
- [23] Y. Zhu, J. Cao, H. Chen, Q. Yu, B. Li, High electrochemical stability of a 3D cross-linked network PEO@ nano-SiO₂ composite polymer electrolyte for lithium metal batteries, *J. Mater. Chem. A* 7 (12) (2019) 6832–6839.
- [24] J. Lopez, D.G. Mackanic, Y. Cui, Z. Bao, Designing polymers for advanced battery chemistries, *Nat. Rev. Mater.* 4 (5) (2019) 312–330.
- [25] Z.-H. Guo, A.N. Le, X. Feng, Y. Choo, B. Liu, D. Wang, Z. Wan, Y. Gu, J. Zhao, V. Li, C.O. Osuji, J.A. Johnson, M. Zhong, Janus Graft Block Copolymers, Design of a polymer architecture for independently tuned nanostructures and polymer properties, *Angew. Chem. Int. Ed.* 57 (28) (2018) 8493–8497.
- [26] A.N. Le, R. Liang, M. Zhong, Synthesis and self-assembly of mixed-graft block copolymers, *Chem. Eur. J.* 25 (35) (2019) 8177–8189.
- [27] K. Kawamoto, M. Zhong, K.R. Gadelrab, L.-C. Cheng, C.A. Ross, A. Alexander-Katz, J.A. Johnson, Graft-through synthesis and assembly of janus bottlebrush polymers from A-branch-B diblock macromonomers, *J. Am. Chem. Soc.* 138 (36) (2016) 11501–11504.
- [28] Y. Xia, B.D. Olsen, J.A. Kornfield, R.H. Grubbs, Efficient synthesis of narrowly dispersed brush copolymers and study of their assemblies: the importance of side chain arrangement, *J. Am. Chem. Soc.* 131 (51) (2009) 18525–18532.
- [29] C. Sinturel, F.S. Bates, M.A. Hillmyer, High χ -low N block polymers: how far can we go? *ACS Macro Lett.* 4 (9) (2015) 1044–1050.
- [30] Y. Luo, B. Kim, D. Montarnal, Z. Mester, C.W. Pester, A.J. McGrath, G. Hill, E.J. Kramer, G.H. Fredrickson, C.J. Hawker, Improved self-assembly of poly(dimethylsiloxane-b-ethylene oxide) using a hydrogen-bonding additive, *J. Polym. Sci. Part A* 54 (14) (2016) 2200–2208.
- [31] A.B. Chang, C.M. Bates, B. Lee, C.M. Garland, S.C. Jones, R.K. Spencer, M.W. Matsen, R.H. Grubbs, Manipulating the ABCs of self-assembly via low- χ block polymer design, *Proc. Natl. Acad. Sci. U.S.A.* 114 (25) (2017) 6462–6467.
- [32] J.-H. Ahn, W.-C. Zin, Structure of shear-induced perforated layer phase in styrene-isoprene diblock copolymer melts, *Macromolecules* 33 (2) (2000) 641–644.
- [33] W. Shan, W. Zhang, M. Huang, Y. Ji, R. Zhang, R. Zhang, Z. Su, H. Liu, X. Feng, D. Guo, Fine-tuned order-order phase transitions in giant surfactants via interfacial engineering, *Giant* (2020) 100002.
- [34] K.M. Abraham, Z. Jiang, B. Carroll, Highly conductive PEO-like polymer electrolytes, *Chem. Mater.* 9 (9) (1997) 1978–1988.
- [35] C. Porter, R. Boyd, A dielectric study of the effects of melting on molecular relaxation in poly(ethylene oxide) and polyoxymethylene, *Macromolecules* 4 (5) (1971) 589–594.
- [36] A.C. Kuo, Poly(dimethylsiloxane), in: J.E. Mark (Ed.), *Polymer Data Handbook*, Oxford University Press, Oxford, 1999, pp. 411–435.
- [37] N.J. Farcich, J. Salonen, P.M. Asbeck, Single-length method used to determine the dielectric constant of polydimethylsiloxane, *IEEE Trans. Microw. Theory Tech.* 56 (12) (2008) 2963–2971.
- [38] E.D. Gomez, A. Panday, E.H. Feng, V. Chen, G.M. Stone, A.M. Minor, C. Kisielowski, K.H. Downing, O. Borodin, G.D. Smith, N.P. Balsara, Effect of ion distribution on conductivity of block copolymer electrolytes, *Nano Lett.* 9 (3) (2009) 1212–1216.
- [39] P.M. Simone, T.P. Lodge, Phase behavior and ionic conductivity of concentrated solutions of polystyrene-poly(ethylene oxide) Diblock copolymers in an ionic liquid, *ACS Appl. Mater. Interfaces* 1 (12) (2009) 2812–2820.
- [40] N.S. Wanakule, J.M. Virgili, A.A. Teran, Z.G. Wang, N.P. Balsara, Thermodynamic properties of block copolymer electrolytes containing imidazolium and lithium salts, *Macromolecules* 43 (19) (2010) 8282–8289.
- [41] I. Gunkel, T. Thurn-Albrecht, Thermodynamic and structural changes in ion-containing symmetric Diblock copolymers: a small-angle X-ray scattering study, *Macromolecules* 45 (1) (2012) 283–291.
- [42] M. Singh, O. Odusanya, G.M. Wilmes, H.B. Eitouni, E.D. Gomez, A.J. Patel, V.L. Chen, M.J. Park, P. Fragouli, H. Iatrou, N. Hadjichristidis, D. Cookson, N.P. Balsara, Effect of molecular weight on the mechanical and electrical properties of block copolymer electrolytes, *Macromolecules* 40 (13) (2007) 4578–4585.
- [43] A. Panday, S. Mullin, E.D. Gomez, N. Wanakule, V.L. Chen, A. Hexemer, J. Pople, N.P. Balsara, Effect of molecular weight and salt concentration on conductivity of block copolymer electrolytes, *Macromolecules* 42 (13) (2009) 4632–4637.
- [44] N.S. Wanakule, A. Panday, S.A. Mullin, E. Gann, A. Hexemer, N.P. Balsara, Ionic conductivity of block copolymer electrolytes in the vicinity of order-disorder and order-order transitions, *Macromolecules* 42 (15) (2009) 5642–5651.
- [45] P. Sutton, P. Bennington, S.N. Patel, M. Stefk, U.B. Wiesner, P.F. Nealey, U. Steiner, I. Gunkel, Surface reconstruction limited conductivity in block-copolymer Li battery electrolytes, *Adv. Funct. Mater.* 29 (48) (2019) 1905977.
- [46] J.P. Coote, T. Kinsey, D.P. Street, S.M. Kilbey, J.R. Sangoro, G.E. Stein, Surface-induced ordering depresses through-film ionic conductivity in lamellar block copolymer electrolytes, *ACS Macro Lett.* 9 (4) (2020) 565–570.
- [47] K. Liu, A. Pei, H.R. Lee, B. Kong, N. Liu, D. Lin, Y. Liu, C. Liu, P.-c. Hsu, Z. Bao, Y. Cui, Lithium metal anodes with an adaptive “Solid-Liquid” interfacial protective layer, *J. Am. Chem. Soc.* 139 (13) (2017) 4815–4820.
- [48] J. Lopez, A. Pei, J.Y. Oh, G.-J.N. Wang, Y. Cui, Z. Bao, Effects of polymer coatings on electrodeposited lithium metal, *J. Am. Chem. Soc.* 140 (37) (2018) 11735–11744.
- [49] X. Kong, P.E. Rudnicki, S. Choudhury, Z. Bao, J. Qin, Dendrite suppression by a polymer coating: a coarse-grained molecular study, *Adv. Funct. Mater.* 30 (15) (2020) 1910138.
- [50] R. Bouchet, T. Phan, E. Beaudoin, D. Devaux, P. Davidson, D. Bertin, R. Denoyel, Charge transport in nanostructured PS-PEO-PS triblock copolymer electrolytes, *Macromolecules* 47 (8) (2014) 2659–2665.
- [51] V. Sethuraman, V. Pryamitsyn, V. Ganesan, Influence of molecular weight and degree of segregation on local segmental dynamics of ordered block copolymers, *J. Polym. Sci. Part B* 54 (9) (2016) 859–864.
- [52] D. Sharon, P. Bennington, M. Dolejsi, M.A. Webb, B.X. Dong, J.J. de Pablo, P.F. Nealey, S.N. Patel, Intrinsic ion transport properties of block copolymer electrolytes, *ACS Nano* 14 (7) (2020) 8902–8914.
- [53] I. Kelly, J. Owen, B. Steele, Mixed polyether lithium-ion conductors, *J. Electroanal. Chem. Interfac. Electrochim.* 168 (1–2) (1984) 467–478.

- [54] L. Yang, J. Lin, Z. Wang, C. Wang, R. Zhou, Q. Liu, Effects of plasticizers on properties of poly(ethylene oxide) complex electrolytes, *Solid State Ion.* 40 (1990) 616–619.
- [55] C.M. Bates, A.B. Chang, N.a. Momčilović, S.C. Jones, R.H. Grubbs, ABA triblock brush polymers: synthesis, self-assembly, conductivity, and rheological properties, *Macromolecules* 48 (14) (2015) 4967–4973.
- [56] D. Rosenbach, N. Mödl, M. Hahn, J. Petry, M.A. Danzer, M. Thelakkat, Synthesis and comparative studies of solvent-free brush polymer electrolytes for lithium batteries, *ACS Appl. Energy Mater.* 2 (5) (2019) 3373–3388.
- [57] Y. Shibuya, R. Tatara, Y. Jiang, Y. Shao-Horn, J.A. Johnson, Brush-first ROMP of poly(ethylene oxide) macromonomers of varied length: impact of polymer architecture on thermal behavior and Li⁺ conductivity, *J. Polym. Sci. Part A* 57 (3) (2019) 448–455.